Map-Driven mmWave Link Quality Prediction with Spatial-Temporal Mobility Awareness

Zhizhen Li, Mingzhe Chen, Gaolei Li, Xi Lin, Yuchen Liu

Abstract—The susceptibility of millimeter-wave (mmWave) links to blockages poses challenges for maintaining consistent high-rate performance. By predicting link quality in advance at specific locations or times of interest, proactive resource allocation techniques, such as link-quality-aware scheduling, can be employed to optimize the utilization of network resources. In this paper, we introduce a map-driven link quality prediction framework that divides the problem into long-term and shortterm link quality predictions to cater to the needs of mobile computing. The first stage aims to predict a long-term radio map considering static network characteristics. We propose to separate LoS and NLoS scenarios, and build an analytical model and a regression-based approach to construct a complete link quality map in the spatial domain. Next, short-term link quality prediction is explored to anticipate future variations in link quality through a spatial-temporal attention-based prediction framework. The essence of this approach lies in capturing the spatial correlation and temporal dependency of mmWave wireless characteristics, followed by an attention mechanism to complement the dynamic link quality prediction task. On top of that, we also design a regional training mechanism with a weighted loss function to address the classical data imbalance problem of map-driven prediction. Extensive experimental and simulation results show that our integrated framework effectively captures comprehensive spatial-temporal knowledge and achieves significantly higher accuracy than other baseline prediction methods, making it a promising solution for a wide range proactive configuration tasks in mobile mmWave networks.

Index Terms—Millimeter wave, link quality, machine learning, spatial-temporal awareness, dynamic prediction.

## I. INTRODUCTION

The development of millimeter-wave (mmWave) technology has garnered considerable interest owing to its capability to deliver high-bandwidth and low-latency wireless communication, effectively meeting the growing demands of mobile applications in 5G/6G cellular networks [1], [2], wireless backhaul [3], [4], Wi-Fi networks [5], [6]. Spanning the frequency range from 30 GHz to 300 GHz, the mmWave bands offer a wealth of available spectrum, enabling the transmission of data at significantly higher rates compared to traditional frequency bands. Particularly, the research community has been actively addressing the technical challenges associated with indoor mmWave communication, aiming to facilitate its

Z. Li and Y. Liu are with the Department of Computer Science, North Carolina State University, Raleigh, NC, 27695, USA (Email: {zli92, yuchen.liu}@ncsu.edu). (Corresponding author: Yuchen Liu.)

M. Chen is with the Department of Electrical and Computer Engineering and Frost Institute for Data Science and Computing, University of Miami, Coral Gables, FL 33146 USA (Email: mingzhe.chen@miami.edu).

G. Li and X. Lin are with the School of Electronic Information and Electrical Engineering, Shanghai Jiao Tong University, Shanghai, China. (Email: {Gaolei\_Li, linxi234}@sjtu.edu.cn).

This work was supported by the U.S. National Science Foundation under Grants CNS-2312138, CNS-2312139, and CNS-2332834.

seamless integration into practical mobile wireless scenarios. On the industry front, standardization efforts such as IEEE 802.11ay [7] and Wireless Gigabit Alliance (WiGig) [8] have been instrumental in defining protocols and specifications for wireless local-area networks (WLANs).

However, the full realization of ubiquitous mmWave communication faces a significant challenge due to its high sensitivity to both static and dynamic blockages. This is attributed to the limited propagation distance and poor penetration capabilities of mmWave signals. Such a problem is exacerbated in obstacle-rich environments, where radio propagation phenomena can be more complex and unpredictable. For instance, in the context of an indoor environment, various factors can affect the quality of mmWave links, including fixed objects and moving humans, leading to prominent multi-path effects, shadowing, and blockages. In this regard, a significant challenge lies in maintaining consistently high link quality amidst the presence of potential blockages and environment dynamics, which necessitates the accurate prediction of link quality at specific locations and times of interest for effective network management. For example, when a mobile user is moving in an indoor environment, the quality of service experienced by mobile users may be significantly enhanced if information about future link quality along the users' routes is used for proactive resource allocation. Furthermore, by leveraging predictive models that incorporate geographical and temporal information of link quality, network operators can make informed decisions enabling the implementation of targeted strategies to ensure reliable communication and improve overall network performance. This motivates the use of map-based link quality prediction, which involves utilizing environmental information to estimate the quality of mmWave wireless links across any location and time, thereby empowering proactive mobile configuration and computation.

While some predictive technologies have been explored in link forecasting [9], they often face limitations due to their inability to comprehensively predict both spatial and temporal aspects. Specifically, existing works tend to focus on predicting link quality between a transmitter and specific receivers, with only a few able to generate link quality maps across desired locations. However, these efforts typically operate under static environmental conditions, lacking exploration into the variations caused by temporary blockages at a map scale, which is the subject of our work. Predicting the mmWave link quality map poses unique challenges in joint spatial-temporal domain, particularly when considering the distinct properties of Lineof-Sight (LoS) and Non-Line-of-Sight (NLoS) scenarios, as well as the impact of dynamic obstacles. To fill this gap, this work proposes a two-stage predictive framework that provides map-driven link quality prediction with contextual awareness,

1

consisting of a long-term prediction mechanism that leverages basic environment information and a short-term predictive model that incorporates spatial and temporal knowledge to handle environment dynamics.

In essence, a high-quality mmWave link always uses a LoS path between the sender and the receiver [10], [11]. When objects made of highly reflective materials such as metal are present in the environment, reflected paths can be also found to maintain high link quality even when no LoS path exists between the two endpoints. As a result, even a minor change in the environmental layout can significantly impact the distribution of LoS and NLoS paths, leading to variations in the quality a mmWave link. This highly environmentdependent nature makes it challenging to achieve accurate predictions, even in static network scenarios. Besides, the dynamic blockages due to moving humans may frequently break this steady state by disrupting the well-established links at different locations, resulting in fluctuations of received signal strength and further making it challenging to estimate the link quality in space and time. Therefore, for accurate prediction of a complete link quality map, it is critical to jointly consider the location of fixed obstacles as well as the effects brought by moving blockers simultaneously.

In this work, we build upon our previous work in [12] focused on long-term link quality prediction by integrating it with a short-term link quality prediction model. As a comprehensive work, in the first stage, we focus on deriving a long-term radio (LTR) map that takes into account the static network characteristics. This map serves as a foundation for a subsequent dynamic short-term prediction, which captures the future variations in link quality within the LTR map. Specifically, for the long term link quality prediction, we leverage a geometric method to separate the LoS and NLoS areas in a given network scenario based on the knowledge of fixed obstacles' sizes and locations. Then, we propose LoS and NLoS link quality predictors using an analytical model and a regression-based deep learning approach, respectively. For the more challenging short-term prediction, a Spatial- Temporal Attention-based Prediction (STAP) framework is developed to capture spatial correlation and learn temporal dependency for predictions in both space and time. We also add a soft attention mechanism to improve the prediction accuracy by learning the importance of the link quality variance at every moment. Specifically, we apply a regional learning method to investigate and tackle the data imbalance problem that exists in the map-driven prediction. We conduct extensive experiments with high quality data covering a wide range of fine-grained mmWave network scenarios, which is generated by elaborated ray-tracing analysis. The results validate the stability, effectiveness, generalization capability, and stretchable time-window prediction ability of our integrated map-driven prediction models. The proposed scheme is also shown to outperform the baseline prediction approaches by up to 61% on the prediction accuracy. It is worth noting that our work is particularly well-suited for semi-dynamic scenarios, such as laboratory or office environments, where some deployed objects are stationary, and human movement represents the primary dynamic blockage to the network.

The specific contributions of this work are as follows.

- We develop for the first time a method to synthetically generate high-quality training data covering a wide range of fine-grained mmWave network scenarios, which is then used to develop a machine learning and regression-based framework, enabling the prediction of link quality at any location, including those that have not been previously visited or measured. Additionally, we investigate a ray-tracing based approach to collect a substantial amount of training data that captures the dynamic environmental changes caused by moving obstacles. This allows for accurate and dynamic prediction of link quality in real-time scenarios.
- We tackle the map-driven link quality prediction problem by dividing it into two sub-problems: long-term radio map prediction and short-term link quality prediction. The long-term prediction framework focuses on capturing the characteristics of the static network environment, allowing for the efficient construction of a complete link quality map. This mainly addresses the impact of static obstacles and permits link quality prediction several seconds into the future to facilitate proactive resource allocation.
- To handle link quality variations under dynamic blockages, we then introduce a spatial-temporal attention-based learning framework for short-term link quality prediction.
   To our knowledge, this is the first work that attempts to integrate temporal dependency and spatial correlation into the map-based mmWave link quality prediction. Such spatial-temporal module enables the predictions over a stretchable time window, providing flexible time ahead for preparedness to proactive countermeasures.
- We perform both simulations and real-world experiments to evaluate our link quality prediction schemes, which show a very good agreement with the ground truths. This demonstrates that mmWave link quality under static and/or dynamic conditions can be accurately predicted through the use of detailed environment information and spatial-temporal characteristics of mobile wireless networks.

### II. RELATED WORKS

Most recent studies have adopted machine learning methods to predict when and where the blockage will happen in mmWave wireless networks [13]. For instance, [14] proposed a recurrent neural network (RNN) architecture based on Gatedrecurrent unit (GRU). The basic idea behind the algorithm is to recognize the pre-blockage signature and predict the incoming blockages. In [13], [15], a vision-aided approach was used to construct a bimodal deep learning algorithm and combine images with mmWave beam for blockage prediction. One main limitation of these approaches is that the blockage does not necessarily cause significant link quality drop as sometimes opportunistic NLoS paths can be found to maintain a high link quality, e.g. when highly reflective obstacles are present nearby. By contrast, our work herein focuses on link quality prediction since that is what drives network management decisions, e.g. AP association, handover, and resource allocation.

Prior works that have addressed the problem considered herein, i.e. link quality predictions in mmWave settings are [9], [12], [16]. [16] adopted a conventional approach to measure the channel state information (CSI) of neighbouring APs to estimate link quality. However, CSI-based link quality prediction is not suitable for mmWave networks since the instantaneous CSI is not always attainable and applicable to predict the link quality at new locations. In our prior work [12], a link quality prediction scheme based on knowledge of the environment is proposed using a deep neural network based predictor. However, this work is limited to estimate the invariant link quality in the static scenario. Particularly, [9], [17] designed long short-term memory (LSTM) models to predict multi-link quality under dynamic blockages. However, these works focused on link quality prediction at a few dedicated locations with considering only temporal-domain information. Recent studies have also tried to utilize generative models to forecast link quality maps [18]. However, these models are limited to predicting link quality maps under static environments. In contrast, our approach jointly considers spatial and temporal domains to predict link quality maps under environment dynamics.

Specifically, spatial-temporal based learning models have been widely applied in the area of traffic flow prediction [19]–[21]. Particularly, [21] built a geographical relation graph according to time series similarity of traffic demand and utilized a graphic recurrent neural network (RNN) and an edge RNN to predict traffic flow data. [20] implemented a convolutional LSTM model to predict travel demand. [22] presented a spatial-temporal learning model and applied transfer learning to tackle data scarcity issue. Nevertheless, spatial-temporal models have not been used for map-based link quality prediction to capture the dependencies between spatial locations and the evolution of the channel over time, which is the subject of our work herein.

The primary challenge we consider in this work is to predict link quality for mmWave networks under NLoS conditions and dynamic blockages. The most relevant works we are aware of that address this problem were [23], [24]. To be specific, [23] adopts a measurement-based approach where link quality measurements are taken as clients move around to different locations and then those measurements are used as predictions for future transmissions at the same locations. While even a very small change in the locations could cause a big difference on the quality of mmWave link, it is impractical to measure every location of a scenario beforehand, thus this approach suffers from not being able to predict link quality at unknown locations or within a entire map. Also, it requires a period of preparation time to collect current measurement data for future prediction. By contrast, our approach can predict link quality at any location by capturing the details of the environment such as locations of obstacles and their reflectivities as well as scenario configurations. To handle dynamic blockage effects, [24] developed a temporal-domain based model to predict the link quality at several fixed location spots in an indoor environment, while our STAP framework in this work captures both spatial correlation and temporal dependency of mmWave wireless characteristics, making it possible to dynamically

construct full link quality maps over time.

## III. SYSTEM OVERVIEW

In this section, we first formulate the problem into two tractable sub-problems: long-term radio map prediction and short-term link quality prediction, followed by an explanation of the technical challenges involved. Then, we present an introduction to the overarching framework.

### A. Problem Statement

To facilitate map-driven link quality prediction in space and time, the geographical area of the environment is partitioned into  $M=N\times N$  grids, in which each grid represents a spatial region  $r_n(1\leq n\leq M)$ . As previously mentioned, our approach to addressing such a problem involves a two-step process, where we first perform long-term radio map prediction that only considers the static environment characteristics with LoS and NLoS division, and then short-term link quality prediction will be augmented to capture the link quality fluctuation caused by potential environment dynamics such as human blockages.

In the first stage, let  $\mathcal{X}$  represents the predicted radio map.  $\bigcup_{i=1}^{N_1} r_i^L$  and  $\bigcup_{i=1}^{N_2} r_i^N$   $(N_1+N_2=M)$  denote the LoS areas and the NLoS areas, respectively. Formally, the long-term prediction problem can be formulated as:

$$\mathcal{X} = \mathcal{F}_1(\bigcup_{i=1}^{N_1} r_i^L) \bigcup \mathcal{F}_2(\bigcup_{i=1}^{N_2} r_i^N), \tag{1}$$

where  $\mathcal{F}_1$  and  $\mathcal{F}_2$  are two different predictors for radio map in LoS areas (L) and NLoS areas (N), respectively.

Second, for the short-term prediction problem, at time step t, we propose to predict  $X^{t+1}$  based on previous T predicted link quality maps  $\mathcal{X}^{t-T:t}=(X^{t-T},\cdots,X^t)$ , where T represents the length of previous time steps. Since we consider the information from both spatial and temporal domains, the prediction problem can be formulated as

$$\hat{X}^{t+1} = \mathcal{F}_3(\mathcal{X}^{t-T:t}, \mathcal{G}^{t-T:t}), \tag{2}$$

where  $\mathcal{F}_3$  is a spatial-temporal predictor and  $\mathcal{G}^{t-T:t}$  denotes the spatial information during the same time period.

## B. Technical Challenges

The major challenges involved in solving the above formulated problem and achieving  $\mathcal{F}_1 - \mathcal{F}_3$  are as follows: 1) The significant disparity between LoS and NLoS link quality in mmWave bands highlights the importance of environmental knowledge for accurate prediction. However, it is analytically challenging to derive link quality based on a variety of complex environmental factors. Specifically, different indoor environments feature various objects composed of different materials, each inducing distinct characteristics of reflections and diffractions on mmWave links. Moreover, the inherent variability in human behavior and movement introduces further unpredictability. Consequently, the compounded effects of both static and dynamic environmental factors render simplistic analytical approaches inadequate for accurately modeling

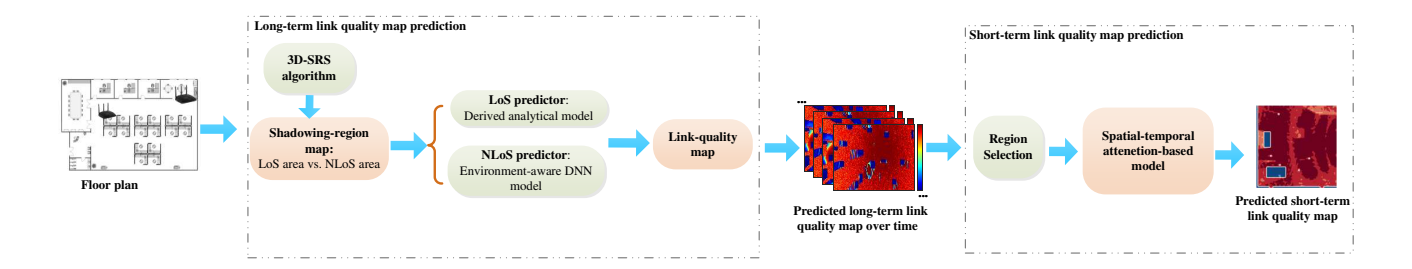


Fig. 1. Architectural overview of map-driven link quality prediction.

this complex phenomenon [25]; 2) Given the substantial influence that minor alterations in transmitter or receiver placement can have on link performance, accurately predicting link quality at new locations without prior measurements is challenging. This becomes particularly difficult when trying to efficiently construct a comprehensive map of link quality that includes unexplored locations; 3) While machine learning techniques can be employed for link quality predictions, obtaining an adequate volume of training data in real-world environments that cover a wide range of complex network scenarios poses a challenge. Collecting large labeled datasets in real-world settings is often prohibitively expensive and impractical due to the significant human effort and complex infrastructure required to accurately capture environmental features and link quality information; 4) In the context of short-term dynamic link quality prediction, a data imbalance problem always arises that adversely affects prediction accuracy. This issue occurs due to the sparse availability of data from areas affected by environment dynamics such as moving objects, while the prediction model receives redundant information from unaffected areas that overshadows the essential information regarding the impact of dynamic changes on link quality.

## C. Solution Overview

Fig. 1 provides a glimpse of our overall map-driven prediction framework that addresses the above challenges. First, a 3dimensional shadowing-region search (SRS) approach is proposed to determine the LoS and NLoS areas of a given network scenario. Second, the region of the entire environment space is partitioned into groups of LoS and NLoS grid locations, which are then fed into the analytical model and trained deep neural network (DNN), respectively. After obtaining the predicted link quality at each location, the complete set of link-quality maps are generated for deployed APs and all possible device heights. Next, to address short-term effects such as moving obstacles that may occasionally "pollute" the derived longterm radio map, we first design a region selection method that learns the impacted area caused by dynamic blockages, and then a spatial-temporal attention-based learning framework is developed to capture spatial correlation and learn temporal dependency for dynamic predictions. In what follows, we discuss the details of technical components in this overall framework.

# IV. LONG-TERM LINK QUALITY MAP PREDICTION

In this section, we present the long-term link quality prediction scheme aimed at constructing a complete radio map based on environment details. These derived maps serve as the foundation for the subsequent short-term prediction augmentation as discussed in Sec. V.

## A. LoS/NLoS Area Determination

The fundamental difference between link quality in the mmWave bands compared to lower frequencies is the sharp difference between the LoS and NLoS cases. We use geometric analysis to identify the shadowed regions in an area that correspond to definite LoS/NLoS cases. Based on knowledge of the sizes and locations of obstacles (i.e., furniture items) in the indoor environment, we propose a 3D shadowing-region search (3D-SRS) approach to efficiently determine the LoS and NLoS areas in a given scenario.

Algorithm 1 summarizes the steps of 3D-SRS algorithm. First, a floor plan of room S at each device height basis  $h_i$  is partitioned into  $N_g$  equal-sized grids with the gridding length of  $l_c$ , where  $\bigcup_{i=1}^{N_g} g_i = S$  and  $\bigcap_{i=1}^{N_g} g_i = \emptyset$ . The algorithm also incorporates obstacle information Obs, including their sizes and locations, and AP locations ap as part of its input. Considering all  $g_i$  in S at the considered device height range H (Lines 1-5), the 2D grid set G and the shadowing-region (SR) map matrix Map are initialized. Next, the virtual heights of obstacles and AP are calculated with respect to different device height bases (Lines 7-8), and then we use the geometric analysis to determine the shadowing-grid set  $SG_i$  given the information of obstacles and AP (Line 9). This geometric algorithm is based on a grid-based shadowing search (GSS) method [10], where the main idea is to check if the center point of a grid element exists in a shadowing polygon formed by an AP and known obstacles. To find all non-overlapped shadowed grids caused by different obstacles, the shadowed-grid set of each obstacle is first derived, and then the intersected grids over different shadowed-grid sets are eliminated. After traversing all known obstacles, the union of SG is obtained. Finally, we add these shadowed (i.e., NLoS) grids into SR-Map for each height basis  $h_i$  (Lines 10-13). The algorithm is terminated after all height bases are traversed.

### B. Data Collection

As mentioned in Sec. III.B, it is not trivial to generate a large training data set with synthetically generated APs of varying

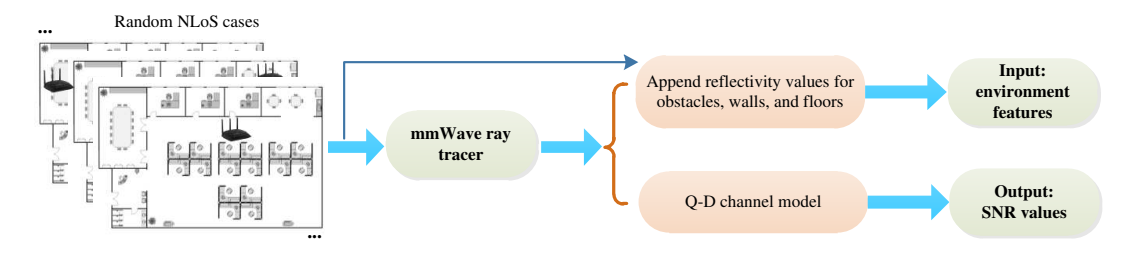


Fig. 2. The overview of FDG framework.

```
Algorithm 1: 3D-SRS: 3D Shadowing-Region Search
   Input: Obs, l_c, N_q, H, ap
   Output: SR-Map
 1 for each height (h_i = H_{min} + i * l_c) \& (h_i <= H_{max}) do
        G(i,:) = [all zeros in floor plan at height h_i];
 2
        init 3D map with all LoS grids
 3
        SR-Map(i,:) = \vec{v}(\text{all zeros, size} = N_q);
5 end
 6 for each height h_i do
        Obs.height = max\{Obs.height - h_i, 0\}; \triangleright change the
 7
         device height basis
        ap.\text{height} = ap.\text{height} - h_i; \triangleright get the virtual height of
 8
         AP w.r.t device height basis
        SG_i = \text{FindSGset}(Obs, ap, G, l_c); \triangleright \bigcup SG_{i,m}
 9
        for each j \in SG_i do
10
            k = SG_i(j);
11
            SR-Map(i, k) = 1; \triangleright NLoS grid location
12
        end
13
14
  end
15 return SR-Map;
```

locations, obstacles of varying sizes, locations, and material properties in arbitrary scenarios. To acquire the large amount of high-quality training data, we introduce the fine-grained dataset generation (FDG) framework as shown in Fig. 2.

Specifically, we first randomly generate various scenario cases with the following features: 1) the lengths, widths, and heights of rectangular room follow uniform distributions L<sub>r</sub>  $\sim \mathcal{U}(10.0, 20.0), W_r \sim \mathcal{U}(5.0, 10.0), \text{ and } H_r \sim \mathcal{U}(2.4, 4.5);$ 2) Objects deployed in the room are modeled as cuboids and placed on the floor, where the center of each obstacle follows a Poisson point process with a specific density  $\lambda$  $\sim \mathcal{U}(0.04, 0.3)$ , the widths, and lengths follow the truncated normal distributions W $\sim TN(0.56, \sigma_w, 0.25, 1.25)$  and L $\sim$  $T\mathcal{N}(1.08, \sigma_l, 0.5, 1.75)$ , where  $\sigma_w \sim \mathcal{U}(0.01, 0.38)$  and  $\sigma_l \sim$  $\mathcal{U}(0.08,\ 0.58)$ . Their heights and orientations follow uniform distributions  $\Theta \sim \mathcal{U}(0, \pi)$  and  $H \sim \mathcal{U}(0.3, 2.3)$ ; 3) each scenario case includes around 50 NLoS user locations, where each randomly-located client (i.e. wireless device) is viewed as a random point, and its height follows the uniform distribution  $\mathcal{U}(0.1, 2.0)$ . These parameters are derived by using a real-life office/lab environment as a guiding example, and all length units of parameters are in meters.

Then, we feed all generated scenario cases into our quasideterministic (Q-D) mmWave ray tracer [26], and do the

following procedures. First, we assign the reflectivity values for obstacles, walls and floor in each scenario, where every obstacle material's reflection loss (dB)  $R_o$  follows the uniform distribution  $\mathcal{U}(0.5, 30.0)$ , the reflection loss (dB) of wall or floor is randomly chosen from the set {5.0, 15.0, 25.0}. The reflectivity parameters are derived based on the actual experiment measurements at 60 GHz from [27]-[29]. Next, these assigned reflectivity values are integrated with the environment information generated from the first step, thus all environment features of each scenario is obtained. In parallel, Q-D ray tracer is used to capture the geometrical properties of the channel for each transceiver and generate the profile of delay  $\tau$ , path gain, angle of departure (AoD)  $\theta_t$ , angle of arrival (AOA)  $\theta_r$ , etc, for the path components in each NLoS case. Any small change in the location of a node translates into changes in these captured profiles.

Lastly, the output results from the ray tracer are directly used as input to a Q-D mmWave channel. Specifically, the Q-D mmWave channel [30] can be characterized using a set of strong reflections and scattering rays, and the channel impulse response is defined as:

$$h(t) = \sum_{\tau} \sum_{\theta_t} \sum_{\theta_r} Y_{tx}(\theta_t) \cdot Y_{rx}(\theta_r) \cdot h(t, \tau, \theta_t, \theta_r)$$

$$= \sum_{i=0}^{N-1} 10^{-PL_i/20} e^{j\phi_i} \cdot (Y_{rx_i} \cdot Y_{tx_i}) \cdot e^{-j2\pi f \tau_i},$$
(3)

where N is the number of generated rays from ray tracer,  $PL_i$  (dB) and  $\phi_i$  are the path loss and phase shift of ray i, and  $Y_{tx_i}$  and  $Y_{rx_i}$  are the radiation pattern of the transmitter and receiver array at ray i, respectively. To be specific, a power spectral representation of the 60 GHz signal is implemented, where the entire channel is divided into a number of equally spaced sub-bands, and each of them has the size of 5.156 MHz corresponding to the sub-carrier spacing for an orthogonal frequency division multiplexing (OFDM) PHY, while in single-carrier (SC) PHY mode, the power is divided equally across all the sub-bands over the entire bandwidth. With the input of the Q-D trace files from mmWave ray tracer, we parse these path profiles to obtain the spatial matrix between every transceiver pair. Specifically, the received power per sub-band  $Rx_i$  is computed and turned into a scalar value to represent the total energy apparent to the receiver by applying RF filtering as in [30], thus the overall received power is obtained by accumulating  $Rx_i$  over all sub-bands, and signal-to-noise ratio (SNR) value is further derived for each NLoS case.

By utilizing this FDG framework, we can effectively generate a large amount of training data including both detailed en-

vironment characteristics and SNR values, paving the way for developing the following regression-based prediction model.

Rather than directly employing the ray tracer to predict the target link quality map, we leverage it to generate a large dataset for training a DNN model, which offers several key advantages. First, once the DNN model is trained offline, it achieves higher computational efficiency. In complex environments, utilizing a ray tracer demands significant computational resources and time. Conversely, a trained DNN can swiftly produce predicted maps in an online manner, enabling real-time applications. Second, employing a DNN allows for the integration of diverse data sources, including environmental factors and link-level characteristics, making the model adaptable for temporal-based predictions at any time instance. This adaptability is challenging to achieve with a ray tracer, which relies on underlying analytical or statistical models. We also present quantitative comparisons in Section VI-A.3.

#### C. Environment-aware Prediction

Here we introduce separate prediction schemes for LoS and NLoS areas. For LoS cases, an analytical model is utilized to estimate the link quality. On the other hand, a more advanced regression-based approach is developed to predict link quality in NLoS locations by capturing intricate environmental details.

1) LoS link-quality predictor: As we know, LoS path component contributes to the majority of link quality at mmWave frequencies (e.g., 60 GHz), which is predominant over NLoS components in the presence of obstacles. Therefore, the link performance under these scenarios is not highly dependent on surrounding obstacles, but instead, depends more on the distance between sender and receiver. Thus, we perform LoS link-quality predictions based on a 3GPP mmWave channel model with parameters chosen for indoor LoS scenarios [31]. To be specific, the path-loss model is derived as:

$$PL = 32.4 + 17.3 \cdot \log_{10}(d_{3D}) + 20 \cdot \log_{10}(f_c) + S_f,$$
 (4)

where  $d_{3D}$  is the separation distance between the transceiver,  $f_c$  is the center frequency normalized by the unit of GHz, and  $S_f$  is the shadowing factor that follows the normal distribution  $\mathcal{N}(0, \sigma_{SF} = 3.0 \text{ dB})$ . In this way, signal-to-noise ratio  $(\mathcal{S})$  can be further derived to quantify the link quality as:

$$S = P_t \cdot G_t \cdot G_r \cdot (10^{PL/10} \cdot N_T)^{-1}, \tag{5}$$

where  $P_t$  is the transmit power,  $G_t$  and  $G_r$  are directional antenna gains at transmitter and receiver, respectively. To be specific,  $G_t$ ,  $G_r$  changes depending on the selected beam and the transmission angle. We set up multiple antenna beam patterns for transmitter, while a single beam pattern for receiver covering a relatively wide range, which aligns with the practical implementation as in [32] as well as our experimental evaluations in Sec. VI. PL is the path loss in Eq. (4), and  $N_T$  is the power of thermal noise. For any given LoS scenarios, we use this log-distance based LoS predictor to estimate the link quality in mmWave WLANs. We also validate the prediction performance of such simple analytical model with both simulations and actual measurements in Sec. VI.

2) NLoS link-quality predictor: When no LoS path exists, the quality of a mmWave is highly dependent on the node placements, locations of surrounding obstacles and their reflectivity properties. Treating these environmental parameters as independent variables and long-term link quality as the dependent variable, a regression-based prediction approach naturally fits this situation. Accordingly, we develop and evaluate a machine learning and regression-based approach to prediction for these cases. By using the FDG data generation framework, we generate large amount of WLAN scenarios and use a mmWave ray tracer to produce ground-truth values of link quality at different locations of each scenario. We use these data to train a DNN to predict link quality under NLoS scenarios.

a) Input feature and output label: We consider the availability of environment information including scenario configuration, obstacle sizes and locations, reflectivity information, the location of AP and client. The input data of DNN model is presented in the format of a concatenated vector  $V_e$ including all environment details. As shown in Eq. (6), for each sample case, the 3D Cartesian coordinates are used to indicate the client position  $\mathcal{U}$ , AP position  $\mathcal{A}$ , and room size  $\mathcal{R}$ .  $\mathcal{N}_o$  represents the number of obstacles and  $\mathcal{O}$  includes the locations, sizes, as well as reflectivities of obstacles. We use the zero-padding method to flatten the obstacle information  $\mathcal{O}$ in different scenario cases. Note that the maximum number of generated obstacles  $N_m$  is equal to  $(\lambda_m \cdot R_{l_m} \cdot R_{w_m})$ , where  $\lambda_m$ ,  $R_{l_m}$ , and  $R_{w_m}$  are the maximum obstacle density and room's length and width as defined in Sec. IV-B. By factoring in all environment details, the input feature vector  $\mathcal{V}_e$  is obtained by concatenating above environment information with the size of  $(6N_m + 12)$ . On the other hand, the output label (ground truth)  $S_r$  used in DNN model is represented in the format of a SNR value. Finally, we post-process the input features and output values through a max-min normalization, which aims to eliminate the impact of scale differences among different features on the regression model.

$$\mathcal{V}_{e} = \{ \mathcal{U}_{(x,y,z)}, \mathcal{A}_{(x,y,z)}, \mathcal{R}_{(x,y,z)}, \mathcal{N}_{o}, \mathcal{O}_{1(x,y,w,l,h,ref)}, ..., \\
\mathcal{O}_{n-1(x,y,w,l,h,ref)}, \mathcal{O}_{n(x,y,w,l,h,ref)}, \mathcal{W}_{ref}, \mathcal{F}_{ref} \}.$$
(6)

b) Network configuration: We use a deep neural network with the number of hidden layers and neurons configured to work across different network scenarios. The flattened input feature vector  $\mathcal{V}_e$  of size  $n_{in}$   $(N_m=60 \text{ from Eq. } (6))$  is fed to a fully connected network with 4 hidden layers as shown in Fig. 3. The  $l^{th}$  hidden layer has a total of  $n_k$  neurons. The  $k^{th}$  neuron in  $(l-1)^{th}$  layer is connected to  $j^{th}$  neuron in  $l^{th}$  layer with a weight of  $w^l_{jk}$ .  $b^l_j$  represents the bias of the  $j^{th}$  neuron in the  $l^{th}$  layer. The activation of the  $j^{th}$  neuron in the  $l^{th}$  layer, i.e.  $a^l_j$ , is calculated through the forward propagation rule as:

$$a_{j}^{l} = \max\{\sum_{k} w_{jk}^{l} a_{k}^{l-1} + b_{j}^{l}, \ 0\}, \tag{7}$$

Next, we use a sigmoid layer before the output layer to transform the output logits to normalized values. The model is trained through the backpropagation rule using a meansquared error loss function. With the available training data

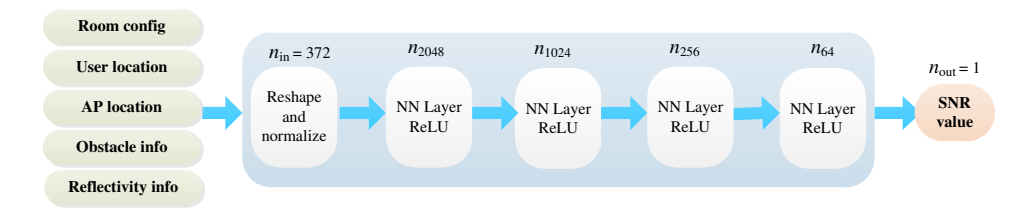


Fig. 3. Model overview with data inputs (green), neural network model (blue), and output (red).

bank,  $DB = \{(\mathcal{V}_{e_1}, \mathcal{S}_{r_1}), (\mathcal{V}_{e_2}, \mathcal{S}_{r_2}), \dots (\mathcal{V}_{e_N}, \mathcal{S}_{r_N})\}$ , of N samples, the loss function is minimized using adaptive moment estimation optimization algorithm. In particular, a batch of B training samples is randomly selected out of N training NLoS sample cases, and the weights  $w_j$  and biases  $b_j$  are updated through the following backpropagation rule:

$$\theta_{t+1} := \theta_t - \frac{\alpha \cdot m_t}{\sqrt{v_t} + \varepsilon} \tag{8}$$

$$m_{t} = \frac{\beta_{1} m_{t-1} + (1 - \beta_{1}) d\theta}{1 - {\beta_{1}}^{t}}, \ v_{t} = \frac{\beta_{2} v_{t-1} + (1 - \beta_{2}) d\theta^{2}}{1 - {\beta_{2}}^{t}}$$
(9)

where a fraction of the gradient in the previous iteration t is retained with the coefficient of momentum, and the hyperparameters  $\beta_1$ ,  $\beta_2$  and  $\epsilon$  are tuned as 0.9, 0.999 and  $10^{-8}$ , respectively. The learning rate  $\alpha$  is initialized as 0.05 and decreased over time with decay factor of 0.9 for each 2,000 iterations, which aims to optimize prediction performance and increasing the convergence rate of the algorithm.

In summary, based on the proposed link-quality predictors that separate LoS and NLoS scenarios, all predicted values at arbitrary locations and device heights can be eventually integrated into a combination of 2-dimensional link-quality maps (as shown in Fig. 1). Note that, although the offline training process for the DNN model is time consuming due to the large amount of data needed to achieve good prediction accuracy, the online prediction process is fairly fast for both the analytical LoS model and trained NLoS regression model, thereby making our long-term prediction solution less time-demanding. Furthermore, the trained model is adaptable to various scenarios, as the DNN can predict the link quality map based on room information. In the event of a room layout change, updating the input to the model allows for the generation of new link quality maps, as illustrated in Fig. 3.

# V. SHORT-TERM LINK QUALITY PREDICTION

Built upon the previously predicted long-term radio map, which encompasses a comprehensive link quality information in the spatial domain, the second step involves forecasting the short-term variations in link quality amid dynamic blockages. In this regard, we introduce a Spatial-Temporal Attention-based Prediction (STAP) framework that seamlessly combines the spatial correlation and temporal dependency of mmWave wireless characteristics within an integrated module, followed by an attention mechanism to complement the overall link quality prediction task. On top of that, we also design a novel regional training approach with a weighted loss function to address the data imbalance problem of map-driven prediction.

## A. Data Collection with Environment Dynamics

While the FDG framework has been specifically designed to collect a substantial volume of training data encompassing a wide range of complex network scenarios, there are challenges in synthetically generating dataset with environment dynamics. This is primarily due to the absence of interfaces that allow for the incorporation of dynamic blockages in the temporal domain. To address this challenge, we employ a commercial ray tracer known as *Wireless Insite*® to introduce moving obstacles and generate dynamic changes in mmWave signal profiles. This tool allows for the accurate simulation of moving obstacles, thereby enabling the realistic generation of dynamic changes in mmWave signal profiles. The tool and data can be found in [33], [34].

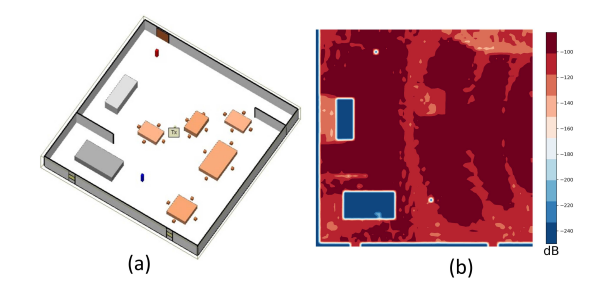


Fig. 4. (a) 3-D scenario layout; (b) The corresponding link quality map.

As an example depicted in Fig. 4 (a), we generate the 3-D layout of an office scenario with a size of 25m×25m×3m, consisting of wooden tables, wooden chairs, metal cabinets, and several moving humans to simulate the dynamic obstacles. The transmitter (i.e., a mmWave access point) is placed at the center of the room with a height of 2.9m, and the receivers are evenly distributed with a spacing of 0.4m and at a height of 1m. Specifically, we choose the 3-D ray-tracing model which has no restrictions on geometry shape or transceiver's height. For a cost-effective ray tracing analysis, the maximum order of reflection paths between a transmitter and a receiver is set to 4, which is a reasonable number in mmWave wireless contexts as the large-order reflection rays have negligible impacts on the overall link quality due to the cumulative reflection loss. Similarly, considering the significant signal strength drop after the first-order diffraction, we set the maximum order of diffraction to reach the receiver as 1. The corresponding link quality map is shown in Fig. 4 (b).

## B. Data Imbalance Problem in Short-term Prediction

Typically, to predict the link quality variance of the entire space, the input of short-term prediction model should be the link quality values at any locations across the previous time steps. However, this straightforward method causes a data imbalance problem, making the prediction model fail to learn useful knowledge brought by the dynamic blockages. Fig. 5 visualizes the difference between the ground truth and the predicted link quality map when the input involves the entire link quality map. While the model accurately predicts link quality in most unaffected areas, we have observed limitations in predicting link quality in blocked areas. This discrepancy can be attributed to the fact that link quality in the majority of areas is generally unaffected by the presence of moving objects.

Typically, common loss functions utilized in deep learning models, such as mean squared error or mean absolute error, assess the global accuracy of the model rather than focusing on local accuracy. Consequently, these models may perform inadequately when dealing with small training samples. For instance, consider two error samples of size 1000:  $\{50,\ldots,50,10,\ldots,10\}$  and  $\{10,\ldots,10\}$ , where the first set includes 100 error samples of 50. The mean absolute errors for these two samples are 14 and 10, respectively. Despite sharing similar mean absolute errors, these two sets of errors exhibit significant differences [35].

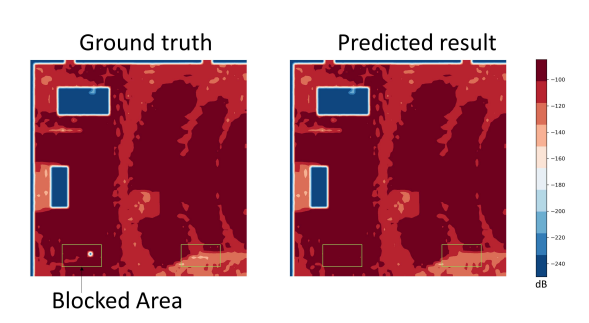


Fig. 5. Comparison between the predicted result with the ground truth using the entire link quality map as the input.

In our considered network scenarios, the size of the unaffected areas often significantly outweighs the affected areas from the temporal perspective. Therefore, even if the model performs poorly in predicting the affected areas, the global error can still be minimal as in [24]. This is due to the fact the amount of valid information obtained from the blocked areas is considerably less than the redundant information retrieved from the unaffected areas. This disparity poses a challenge for the data training model in effectively capturing critical information about the dynamics of the environment. Consequently, it becomes necessary to shift attention towards the link quality variance in the areas surrounding dynamic obstacles.

To address this problem, we propose a regional learning mechanism that strategically considers the link quality status of adjacent regions of the moving obstacles as input to the prediction model during the training process. This can be viewed as a data under-sampling method that reduces the samples from those unaffected areas. As shown in Fig. 6, the selected area can be a rectangle region of arbitrary size, covering the neighboring area of the potential obstacles. It is worth noting that the size of the selected region is a tunable

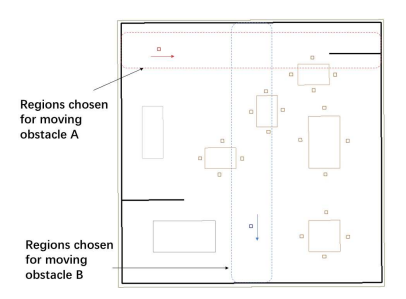


Fig. 6. Regions selected for short-term link quality prediction.

parameter and we evaluate the impact of the region selection on the prediction performance in Sec. VI-B. Besides, during the back propagation process, a weighted loss function is designed to further address this data imbalance issue. Traditional loss functions using basic mean absolute error (MAE) are inappropriate for our problem since the error is always small as long as the link quality is well predicted in those unblocked areas. To resolve this problem, we use the loss function with a penalty parameter  $\gamma$  as follow:

$$\mathcal{L}_{\delta} = \frac{\sum_{i=1}^{n_1} |y_i - \hat{y}_i| + \sum_{j=1}^{n_2} \gamma |y_j - \hat{y}_j|}{n_1 + n_2}, \quad (10)$$

where  $y_i$   $(y_j)$  and  $\hat{y_i}$   $(\hat{y_j})$  represent the ground-truth value and the predicted value of link quality in the unblocked (blocked) areas, respectively. Hyper-parameter  $\gamma$  is set as 10 during training.

# C. STAP Framework

In this part, we present the proposed STAP framework for link quality predictions. As shown in Fig. 7, we first design a graph convolutional network (GCN) to extract the spatial-domain features of mmWave wireless environment from the long-term radio map, and then a long short-term memory (LSTM) based module is used to capture the temporal dependency for predicting link quality variance in future time steps. We also add a soft attention mechanism by assigning weights to the past time-series data to further improve the prediction accuracy.

1) Spatial-domain Correlation: In a dynamic mmWave wireless environment, the presence of moving obstacles can easily affect the link quality between transceivers at arbitrary locations. Thus, it is necessary to capture the spatial correlation between link quality variance and environment details. To this end, we first partition the space (as shown in Fig. 4 (a)) into many grids and place a receiver at each grid to record the received signal strength during our ray tracing analysis. That way, each receiver can be regarded as a vertex and assuming that the neighboring vertices of the receiver are highly correlated, we then add the edges between these neighbouring vertices to further construct a connected graph which contains detailed spatial information.

Next, we use two layers of GCN model to extract spatialdomain features, taking into account the graph node and the adjacent links of the node to capture the correlation between

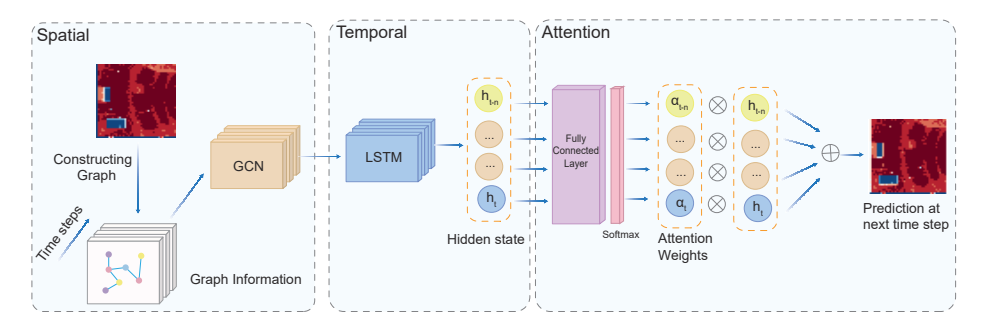


Fig. 7. Overview of the spatial-temporal attention-based prediction framework.

link quality and environment details. A multi-layer GCN can be expressed as:

$$H^{(l+1)} = \sigma(\tilde{D}^{-\frac{1}{2}}\hat{A}\tilde{D}^{-\frac{1}{2}}H^{(l)}\theta^{(l)}), \tag{11}$$

where  $\hat{A} = A + I$ , A is the adjacency matrix of the constructed graph, and I is the identity matrix.  $\tilde{D}$  is the degree matrix with  $\tilde{D}_{ii} = \sum_{j} \hat{A}_{ij}$ .  $H^{(l)}$  is the output of the layer l.  $\theta^{(l)}$  is the parameter of the layer l, and  $\sigma$  is the activation function.

In the stage of graph convolution, each node will combine the information received from its neighbouring nodes and then share the learned knowledge with each other. In this way, our GCN model encodes the topological structure of the graph and captures the spatial correlations among all nodes and links.

2) Temporal-domain Dependency: To learn the temporal dependency of link quality variances caused by blockages and multi-path effects along the timeline, we use a LSTM layer in the framework to predict the received signal strength at any locations of a future time step. The rational behind selecting LSTM model lies in its architecture's ability to sequentially process data, making it well-suited for time-series analysis of link quality over time. This is especially relevant in dynamic scenarios where link quality at each location exhibits both long-term and short-term dependencies. For instance, values at distant locations to the moving obstacles may remain relatively stable, whereas those closer points are subject to frequent fluctuations. The LSTM model's capability to capture and learn from these temporal dependencies ensures accurate prediction and analysis of link quality in the face of changing network conditions. Particularly, as a variant of recurrent neural network, LSTM is further designed to circumvent the vanishing gradient problem that prevents the network to learn time dependency in long sequence data. This feature is especially pertinent to our study, where discerning the impact of short-term disturbances on the long-term link quality map is crucial. In essence, the model includes the forget gate, input gate and output gate, where the memory cell combines the previous cell states, current input and previous output, to update hidden states. The forget gate determines whether the link quality information in the previous memory should be discarded or not. The output gate learns how the memory cell should affect the hidden states. As such, this LSTM layer can well predict the link quality of the future time step based on the previous hidden state information and the input at the current time step, which captures the dynamic temporal variations with such a gated mechanism.

3) Attention-based Enhancement: As the last component in Fig. 7, we add a soft attention layer in the STAP framework to learn the importance of the link quality at every moment. Since each past data in both space and time will have a different degree of impact on the link quality in future time steps, it is critical to strategically assign different weights to those historical data pieces for a more accurate prediction.

To be specific, suppose that the input time series is  $X = \{x_1, x_2, \ldots, x_n\}$ , then for every single time step  $x_k$  in X, there is a corresponding hidden state  $h_k$  from the LSTM output. Typically, the hidden state  $h_n$  of the last input time step is used as the output for prediction. However, the information from much earlier time steps might not be totally ignored or addressed as it may also contain some important knowledge that contributes to the prediction at next time steps. In this way, the output of the attention layer is calculated in a weighted average way as:

$$\hat{h} = \sum_{i=n}^{n} \alpha_i h_i, \tag{12}$$

where  $\alpha_i$  is the weight of each hidden layer. To calculate the weights, we train a fully connected layer on the hidden states to get a score for each state as follow:

$$s_i = sigmoid(w^T h_i + b_i), \tag{13}$$

where  $s_i$  is the calculated score. Then, we use a softmax function in Eq. (14) to normalize this score and get the weight for each hidden state.

$$\alpha_i = \frac{exp(s_i)}{\sum_{k=1}^n exp(s_k)},\tag{14}$$

In summary, the integrated framework comprising the long-term radio map prediction (Sec. IV) and short-term link quality prediction (Sec. V) effectively captures the characteristics of the static network environment in the spatial domain and the dynamic impacts on link quality in the temporal domain, allowing for the efficient construction of a complete link quality map with spatial-temporal awareness. In practice, the network designer only needs to train the long-term prediction model for one time, then the pre-trained model can be easily transferred whenever the placement of object changes or the input is a new scenario. What's more, an online learning method can also be adopted for our short-term link quality prediction model whenever new link quality data is received. In all, this framework paves the way to design *anticipatory* 

networking approaches for future wireless systems, e.g., performing proactive AP association/handover combining the link quality prediction with the user mobility information, and/or allowing the scheduler to adaptively schedule links when their quality is expected to be high. We will leave these promising directions as the future work.

## VI. EVALUATION RESULTS

In this section, we evaluate the performance of our mapdriven link quality prediction framework, which comprises both the long-term radio map prediction and the short-term STAP mechanism through a combination of simulations and actual experiments.

# A. Long-term Link Quality Prediction

1) Performance of LoS link quality predictor: First, we evaluate the performance of our analytical LoS prediction model. We generate various LoS cases and obtain the ground-truth SNR values by using the FDG framework. Then, we use the approach derived in Sec. IV to estimate the link quality for each LoS case, and the results are reported in Fig. 8.

Fig. 8 shows the comparison between the predicted SNR and ground truth at different user locations. As expected, we observe that link quality values are fairly high under LoS conditions, falling within a narrow range of 40–50 dB. On the other hand, it is noted that the gap between the predicted results and ground truths is quite small – the average SNR results are 45.54 dB and 46.12 dB, respectively (power of thermal noise is  $7.04 \times 10^{-12}$  Watts). This result demonstrates the feasibility of the log-distance based model to estimate link quality in LoS scenarios of mmWave WLAN, because the LoS path dominates the link quality at mmWave frequencies, which makes it mainly dependent on the separation distance between the sender and receiver rather than on the surrounding obstacles.

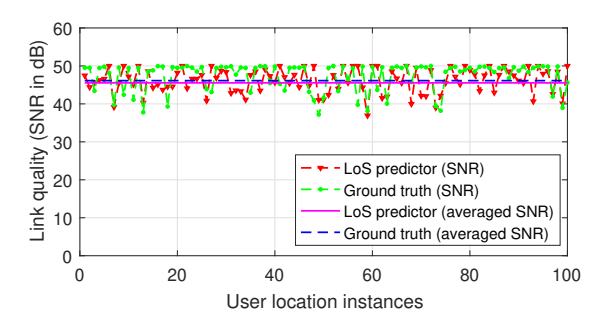


Fig. 8. Link quality prediction comparison for LoS cases.

2) Performance of NLoS link quality predictor: Here, we evaluate our link quality prediction approach for the challenging NLoS cases, which are highly dependent on environment characteristics. We spend several months generating 600,000 data samples using our dataset generator (see Sec. IV-B)<sup>1</sup>, split the data into two sets, and conducte cross validation,

where the training set is comprised of 90% of the data to learn the neural network parameters, and the remaining 10% of the dataset is used for validation and testing. We use TensorFlow and an NVIDIA P100 GPU to implement our DNN-based regression model, which is then used to predict the link quality in new instances, and we calculate the performance difference ratio (PDR) to measure the difference between the predicted values and ground truths. The PDR is defined as  $|\mathcal{S}_{pred} - \mathcal{S}_{truth}|/(\mathcal{S}_{max} - \mathcal{S}_{min})$ , where the denominator represents the difference between the maximum SNR and minimum SNR observed across all test data samples.

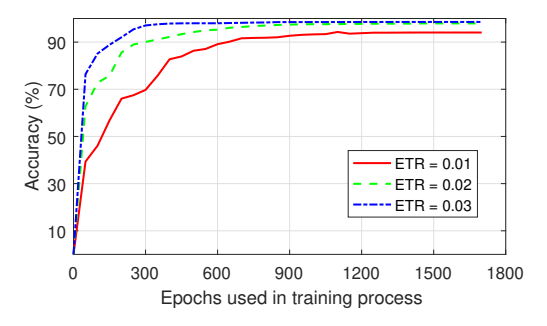


Fig. 9. Prediction accuracy vs. number of training epochs.

First, we evaluate the prediction accuracy with varying *error* tolerance rate (ETR), where the predicted link quality  $S_{pred}$  is accepted as an accurate result when the PDR is less than the given ETR. Fig. 9 shows the prediction accuracy vs. the number of training epochs for different ETRs. As expected, the accuracy becomes higher as the number of epochs used to train the DNN model increases, where the prediction accuracy can achieve 93.86%, 97.89% and 98.54% for different ETRs with a sufficiently large number of epochs. On the other hand, a larger ETR provides a higher prediction accuracy and converges faster, which indicates that most predicted values can efficiently approximate the ground truth during the regression process.

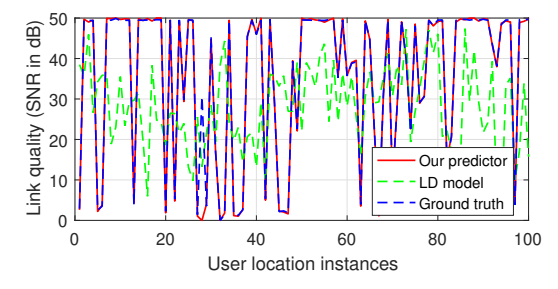


Fig. 10. Link quality prediction comparison.

Second, we evaluate the performance of our predictor for discrete instances within a mmWave WLAN. Here, we also report results for the log-distance based (LD) model from 3GPP Release 16 [31] as a comparison point. Fig. 10 shows the link quality results at different user locations. As compared to the results of LoS cases in Fig. 8, we observe that link quality fluctuates within a wider range due to its high environment dependency. When we examine the results of 3GPP LD model, the estimated link quality typically falls within a relatively narrower range of 15–35 dB, and over 70% of data instances

<sup>&</sup>lt;sup>1</sup>Note that this data generation time is not a serious issue, because it only has to be done once to generate the model and then it can be used as many times as needed for different room and obstacle environments.

underestimate the link quality in evaluated cases. However, the predicted link quality from our predictor matches the ground-truth data well since it accounts for the environment characteristics.

3) Link-quality map construction: In this part, we evaluate the performance of our combined LoS and NLoS predictors to produce link-quality maps for a given network scenario. Fig. 11(a) shows a WLAN scenario with several obstacles and two APs deployed. We run our ELP framework to generate 2-dimensional link-quality maps for each AP and each possible device height. Fig. 11(b) and Fig. 11(c) show the two corresponding link-quality maps for a device height of 0.8m. With the maps of link quality, one can easily find the link quality at any location of a given scenario.

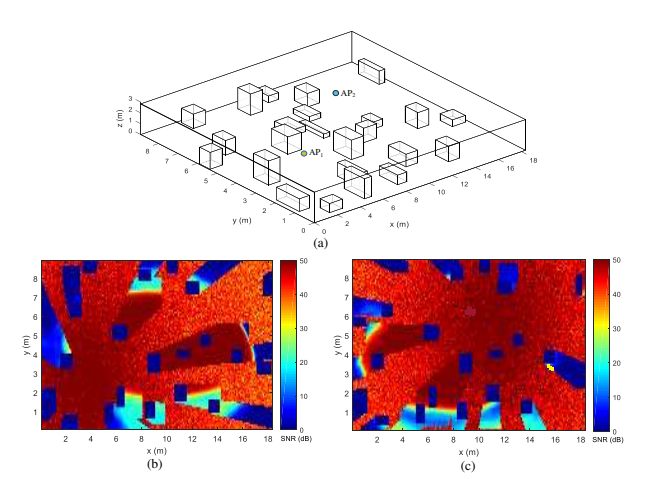


Fig. 11. (a) Scenario example; (b)-(c) Link-quality maps for  $AP_1$  and  $AP_2$  (device height is 0.8m).

It is worth noting that, using our ELP framework, only 10.58 minutes are needed to generate the complete set of link-quality maps for two APs and all possible device heights (with gridding length of 0.1m) in the evaluated scenario.<sup>2</sup> In contrast, to generate one 2-D map, i.e. for one AP and one device height, a full ray-tracing calculation took more than two weeks. Therefore, constructing all maps using ray tracing is not practical since this would require more than 3 years of computation time for the given scenario.

4) Discussion of required environment information: Our link quality predictor requires the input of some environment details, including locations, sizes, and material reflectivities of surrounding objects in a given scenario. In practice, objects' locations, sizes, and material types could be obtained in a variety of ways, e.g., through camera-based sensing, but it is non-trivial to get the exact reflectivity values of different objects. The reflectivity index can be estimated based on the knowledge of object material types from reported measurements, e.g. [27]–[29]. Because these values will not always match the actual reflectivities of objects in a given environment, in this subsection, we evaluate the robustness of our prediction framework to deviations of the reflectivity values.

Here, we add random noise to the reflectivity values of obstacles, walls, and the floor. The noise, which follows a normal distribution  $\mathcal{N}{\sim}(0,\ var)$  in dB units, is added to the actual reflectivity loss chosen as described in Sec. IV. The disturbed reflectivity values combined with other required information are fed into our predictor while the undisturbed values are used for the ground truth calculation. We re-ran the accuracy evaluations from Sec. VI-A to see how the variation of reflectivity values affects the link quality predictions.

Fig. 12 shows the prediction accuracy vs. different variances for the reflectivity noise values. Compared to the baseline with 0 dB variance, we observe that there is almost no impact on the accuracy performance with 1 dB of noise variance. When increasing *var* to 3 dB and 5 dB, the accuracy performance only degrades 1.6%–3% for ETR of 0.01 and 0.5%–2.5% for ETR of 0.03, respectively, which validates the robustness of our prediction method to the reflectivity inaccuracies. Thus we conclude that our proposed approach can tolerate reasonable deviations on the estimated reflectivity values, and maintain a good prediction accuracy without the need for exact reflectivity information.

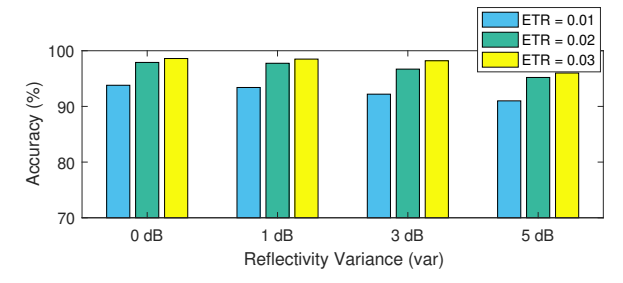


Fig. 12. Prediction accuracy vs. reflectivity variance.

5) Experimental validation: To further validate the performance of our link quality prediction, we performe real-world measurements of link quality in an actual network environment and compare them to the predicted values.

Fig. 13(a) and (b) give an overview of the laboratory setup. Specifically, we conducte the experimental measurements in a 10m×6m×3m laboratory environment, and a TP-link Talon ad7200 router mounted on the ceiling is used as the AP. The Talon router contains the Qualcomm QCA9500 chipset, which implements the IEEE 802.11ad standard. Then, we use an Acer Travelmate P648 laptop as a client device to communicate with the AP. We measure the PHY-layer link quality (SNR) at different locations using the Linux iperf3 and iwconfig tools. The entire laboratory scenario is precisely modeled with a number of cuboid-based obstacles as shown in Fig. 13(c), and we extract the required environment features as the inputs to our link-quality predictor, which then generates the predicted values. We consider 20 user locations that consisted of 5 LoS cases and 15 NLoS cases. The performance comparisons between the prediction and measurement are reported in Fig. 14 and Fig. 15.

Fig. 14 shows the results of LoS scenarios, and it is observed that the predicted values are very close to the actual measurements at different LoS locations, with differences of only around 0.5–2 dB. This result is not surprising since the

<sup>&</sup>lt;sup>2</sup>The running time is evaluated on an Intel(R) Core(TM) i5-6200U 2.3GHz CPU workstation with 2 cores and 4 logical processors.

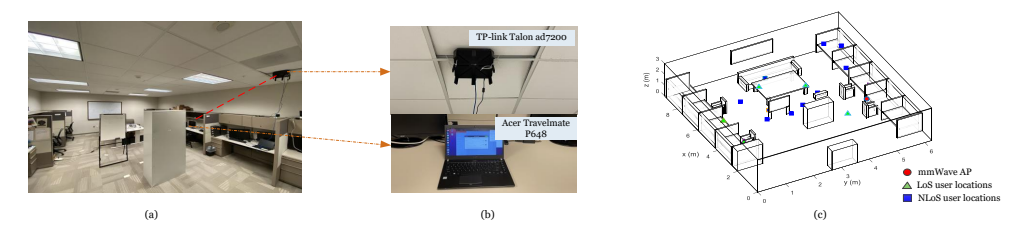


Fig. 13. (a) Network scenario; (b) 802.11ad AP and client laptop; (c) Modeled scenario and measured users.

link quality is consistently high when there is a LoS path between the AP and the client.

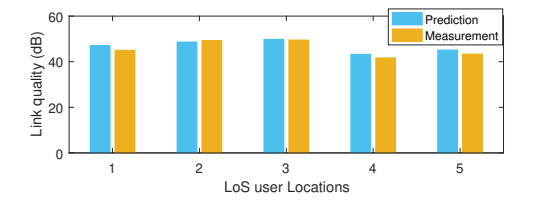


Fig. 14. Link quality validation of LoS locations.

For the NLoS cases in Fig. 15, we observe that the link quality is typically different at each location due to the changes in surrounding obstacles, but our predicted results can still achieve a good agreement with the measurement data. For instance, at locations #1, #5 and #12, high link quality is predicted since the client is located near a metal cabinet in the scenario. While extremely low link quality is predicted and observed at locations #2, #8 and #9 due to the long distance and lack of highly reflective objects nearby. Here the predicted values fairly consistently overestimate the link quality by about 3-5 dB, and we think this is due to the lack of a precise transmission power given in the specifications of the Talon AP used in the measurement. For prediction purposes, we chose a middle value within the specified transmission power range to train our predictor. However, with a calibration of around 4 dB, the differences can be reduced to achieve very close agreement with the actual measurement results. In summary, due to the significant alignment observed between the predictions obtained from simulations and the actual measurements, in what follows, we choose to primarily focus on performance validation in our simulation environment for the sake of simplicity.

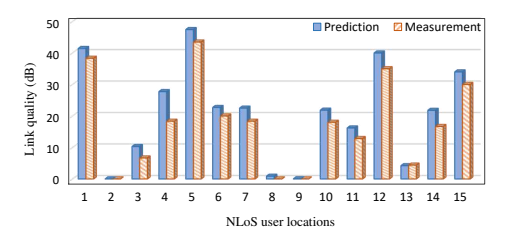


Fig. 15. Link quality validation of NLoS locations.

## B. Short-term Link Quality Prediction

1) Impact of region selection: As described in the Sec. V-B, we exploit a regional learning mechanism to overcome

the data imbalance issue in short-term link quality prediction. Intuitively, considering a large region size in the model may compromise the prediction personalization, resulting in the increase of the local MAE, while a small region size will fail to capture the sufficient spatial information for prediction due to the high environment dependency of mmWave links. Therefore, it is utmost of importance to choose an appropriate region size in our STAP framework.

In this part, we evaluate the performance of STAP model with different region sizes and the results are reported in Fig. 16. First, it is expected to see that the global MAE increases with the larger region size due to the data imbalance issue. Then, it is interesting to observe that the local MAE decreases at first, but then starts to increase as the considered region size becomes larger. The initial decrease is due to more spatial information being considered as the selected area is expanded. However, as the region size keeps increasing, the data imbalance begins to dominate and overwhelm the benefits brought by spatial information, resulting in higher local MAE. In what follows, we select the 11% of the space size for regional learning because it strikes a good balance between the local MAE and the global MAE.

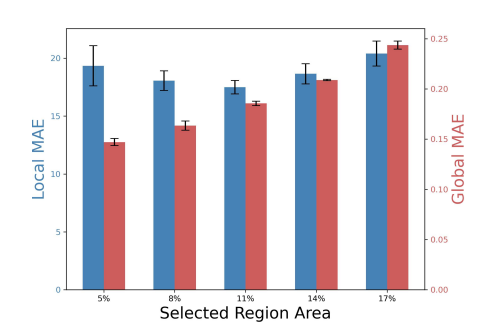


Fig. 16. Area percentage of selected region vs. MAE.

2) Model comparison: Next, to validate the performance of our proposed STAP model, we compare with several baseline models including LSTM based model from [24], CNN-LSTM model from [20], GCN-LSTM model from [36], and the STAP model using the standard MSE based loss function (termed as STAP-STD), while our proposed STAP herein is trained with a modified loss function  $\mathcal{L}_{\delta}$  in Eq. (10).

Table. I shows the performance comparisons among all considered models. Obviously, the proposed STAP outperforms other baseline models in terms of both global MAE and local MAE. By capturing the spatial dependency information, our STAP, CNN-LSTM and GCN-LSTM can improve the prediction accuracy by up to 61%, 24%, and 39% compared to the

TABLE I PERFORMANCE COMPARISONS.

Method	MAE	
	Local MAE	Global MAE
LSTM [24]	41.7542	0.2652
CNN-LSTM [20]	31.7453	0.2781
GCN-LSTM [36]	25.1281	0.2548
STAP-STD	18.1567	0.1922
STAP	16.1409	0.1902

pure LSTM, respectively, which demonstrates the importance of spatial correlations in mmWave link quality prediction. In addition, our STAP is superior to GCN-LSTM and CNN-LSTM by adding a soft attention mechanism, which considers the correlation between links in both space and time. We also find that the STAP shows the better performance than STAP-STD, and this validates the effectiveness of the modified loss function that well addresses the data imbalance issue.

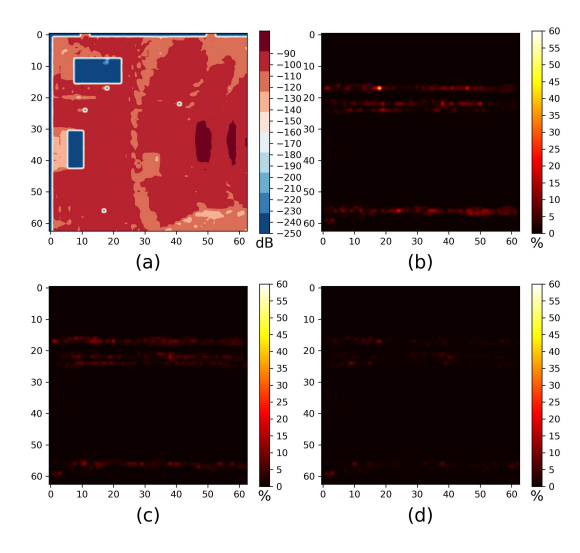


Fig. 17. Visualization of prediction results. (a) is the predicted link quality map of STAP; (b)-(d) are the error maps between predicted and ground-truth link quality maps from LSTM, GCN-LSTM, and our STAP models.

Besides the quantitative results presented in Table. I, Fig. 17 depicts the visualized map-driven prediction results. Specifically, we showcase the prediction error map (i.e.,  $\forall i \in L$ ,  $|\hat{x}_i - x_i|/x_i$ ) for each model, where  $\hat{x}_n$  and  $x_i$  are the predicted and ground-truth link quality at any location  $i \in L$ . The brighter pixel in the map indicates the larger prediction error, so the superiority of STAP model can be easily observed, which is consistent with the quantitative results in Table. I. Additionally, as discussed in Sec. III-C, we only predict the future link quality of the neighbouring area of obstacles. The link quality of the remaining area is the same as that of the last time step. As what we find from the error maps in Fig. 17(b)-(d), the majority of the error in those areas are around zero, which means the link quality from last time step is almost the same as the next time step. This result validates the effectiveness of our regional learning mechanism, namely achieving high prediction accuracy with less computational overhead.

Additionally, we evaluate the response time across different models, and the results are shown in Fig. 18<sup>3</sup>. As expected, the system response time of all three models increases with human density due to the need to process more positional information when multiple objects are included. We observe that the pure LSTM model achieves the fastest response time because it does not consider spatial information, resulting in lower link quality prediction accuracy as shown in Tab. I. In contrast, our STAP model, which integrates both spatial and temporal information, exhibits only a marginal increase in response time compared to the LSTM model - approximately 1 ms. Given the superior accuracy performance of our STAP model, this minor increase in response time is a worthwhile trade-off. As a comparison point, the CNN-LSTM scheme demonstrates the longest response time, attributable to the intrinsic structure of the CNN model, where each node must aggregate information from a fixed number of neighboring nodes. In our STAP framework, nodes only receive information from useful connected nodes, thereby reducing processing delay.

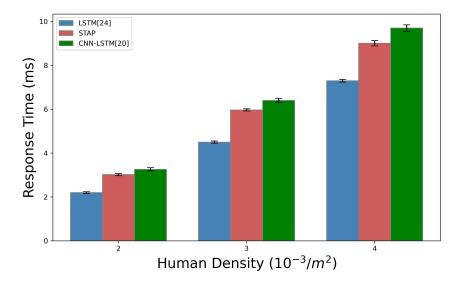


Fig. 18. System response time of different models.

3) Prediction on stretchable time windows: In addition to predicting the link quality at only the next time step, our STAP model is capable of making predictions on a stretchable time window, i.e., generating link quality maps for next several time steps, where each time step is set as 30ms in this evaluated case. Here we first investigate the performance of our STAP model vs. the future time steps in Fig. 19(a). As expected,

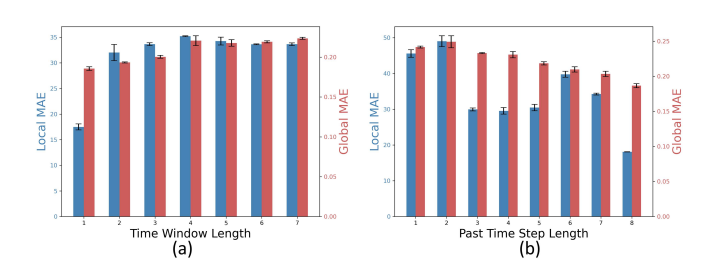


Fig. 19. (a) The length of future time window vs. MAE; (b) The length of past time window vs. MAE.

the prediction error increases when the model becomes more farsighted. Additionally, we observe a significant increase of local MAE at first, but then it becomes marginal as the time step increases. Notably, both local and global MAE stay almost unchanged when the window length is larger than 4, where the global prediction error is maintained at around only

<sup>&</sup>lt;sup>3</sup>The running time is evaluated on an Intel(R) Core(TM) i9-13900 5.6GHz CPU workstation with 24 cores and Nvidia(R) RTX(TM) 4090 GPU.

0.22. This result demonstrates the capability of our STAP model to predict link quality within a stretchable time window, exhibiting the potential use to allow for proactive network configurations in different delay-sensitive applications.

Besides the study on the "lookahead" capability, here we use the term "lookback" to depict length of past time step needed for predicting the future link quality. Intuitively, a longer lookback period can encode more temporal information during the learning process, thus improving the prediction accuracy. This hypothesis is proved in Fig. 19(b), where we can see a decreasing trend in both local MAE and global MAE when more lookbacks are considered. Specifically, the prediction error becomes relatively small when the lookback period is more than 3 in the evaluated scenario. As a result, we conclude that the information from a few past time period might be sufficient to make an accurate link quality prediction.

4) Impact of dynamic blockage density and model generalizability: In this part, we evaluate the performance of our STAP model with varying moving human density in the network scenario. Fig. 20 shows the PDR metric vs. the moving human density. We adopt different ETRs to evaluate the performance of the proposed prediction model, where the predicted link quality is accepted as an accurate result when the PDR is less than the given ETR. As expected, the increase of human density will cause a decrease in the percentage of accepted prediction results across all receiver locations in the scenario. However, our STAP model can still maintain around 85% and 97% prediction accuracy with a large dynamic blockage density when ETR is 0.01 and 0.03, respectively, which corresponds to the average link quality prediction error of just 1-3 dB across the entire scenario map. The results validate the stability of our proposed model, i.e., being able to predict the link quality variance within an acceptable accuracy as the density of dynamic blockages increases.

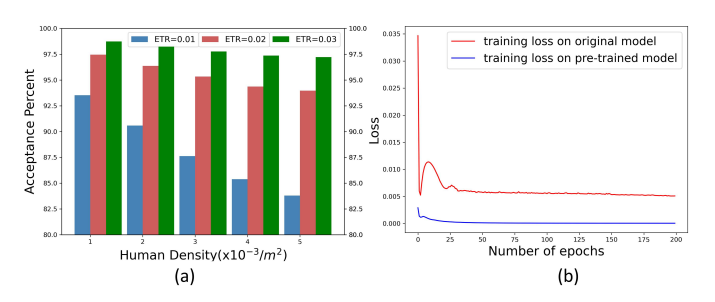


Fig. 20. (a) Prediction accuracy vs. moving obstacle densities; (b) Loss comparison on original model and pre-trained model.

Lastly, we investigate whether our STAP model is generalized to arbitrary mobility patterns of temporary obstacles. We evaluate the model performance in the case of humans moving in random directions, and the results are reported in Fig. 20. Specifically, the red line in Fig. 20 represents the learning loss vs. the used epochs when training a new model, while the blue line shows the convergence when new dataset consisting of a different moving pattern is used as input to a pre-trained model. In particular, it is observed that the initial loss on the pre-trained model is significantly lower than that of the newly trained model. Also, adding the new data to our pre-trained model converges faster and achieves the lower loss. This result

shows the generalizability of our model to mobility pattern of obstacles, which can be applied in various dynamic mmWave network scenarios, since only a few epochs are needed to train a link quality predictor based on the pre-trained model.

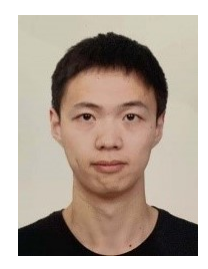
## VII. CONCLUSION

This paper focused on addressing the map-driven mmWave link quality prediction problem. We presented a comprehensive approach that involves dividing the problem into long-term and short-term link quality prediction. For the long-term link quality prediction, we separate the LoS and NLoS cases and design two corresponding predictors to construct a complete radio map based on the environment details. In terms of short-term link quality prediction under dynamic blockages, we tackle the challenge of data imbalance by introducing a regional learning mechanism. This mechanism enables effective training of a spatial-temporal attention-based model using a synthetically generated dataset. Extensive evaluation and experimental results demonstrated that our approach can achieve fairly promising prediction accuracy and is robust to multiple dynamic obstacles with arbitrary mobility patterns.

#### REFERENCES

- V. Velez, J. P. Pavia, N. Souto, P. Sebastião, and A. Correia, "Performance assessment of a RIS-empowered post-5G/6G network operating at the mmWave/THz bands," *IEEE Access*, 2023.
- [2] W. Jiang and H. D. Schotten, "Initial beamforming for millimeter-wave and terahertz communications in 6g mobile systems," in *IEEE Wireless Communications and Networking Conference (WCNC)*. IEEE, 2022.
- [3] M. Kandasamy, N. Yuvaraj, R. A. Raja, N. Kousik, M. R. Tf, and A. S. Kumar, "QoS design using Mmwave backhaul solution for utilising underutilised 5G bandwidth in GHz transmission," in 2023 Third International Conference on Artificial Intelligence and Smart Energy (ICAIS). IEEE, 2023, pp. 1615–1620.
- [4] Y. Liu, Q. Hu, and D. M. Blough, "Joint link-level and network-level reconfiguration for mmWave backhaul survivability in urban environments," in *Proc. of ACM Conference on Modeling, Analysis and Simulation of Wireless and Mobile Systems*, 2019.
- [5] Y. Jian, M. Agarwal, S. K. Venkateswaran, Y. Liu, D. M. Blough, and R. Sivakumar, "Wimove: Toward infrastructure mobility in mmwave wifi," in *Proceedings of the 18th ACM Symposium on Mobility Man*agement and Wireless Access, 2020, pp. 11–20.
- [6] Y. Liu, S. K. Crisp, and D. M. Blough, "Performance study of statistical and deterministic channel models for mmwave wi-fi networks in ns-3," in *Proceedings of the 2021 Workshop on ns-3*, 2021, pp. 33–40.
- [7] Y. Ghasempour, C. R. Da Silva, C. Cordeiro, and E. W. Knightly, "IEEE 802.11 ay: Next-generation 60 GHz communication for 100 Gb/s Wi-Fi," *IEEE Communications Magazine*, vol. 55, no. 12, pp. 186–192, 2017.
- [8] T. Nitsche, C. Cordeiro, A. B. Flores, E. W. Knightly, E. Perahia, and J. C. Widmer, "IEEE 802.11 ad: directional 60 GHz communication for multi-Gigabit-per-second Wi-Fi," *IEEE Communications Magazine*, vol. 52, no. 12, pp. 132–141, 2014.
- [9] S. H. A. Shah and S. Rangan, "Multi-cell multi-beam prediction using auto-encoder LSTM for mmwave systems," *IEEE Transactions on Wireless Communications*, vol. 21, no. 12, pp. 10366–10380, 2022.
- [10] Y. Liu, Y. Jian, R. Sivakumar, and D. M. Blough, "Maximizing line-of-sight coverage for mmWave wireless LANs with multiple access points," IEEE/ACM Transactions on Networking, vol. 30, no. 2, 2021.
- [11] Y. Jian, M. Agarwal, Y. Liu, D. M. Blough, and R. Sivakumar, "Poster: Hawkeye-predictive positioning of a ceiling-mounted mobile ap in mmWave WLANs for maximizing line-of-sight," in *The 25th Annual International Conference on Mobile Computing and Networking*, 2019.
- [12] Y. Liu and D. M. Blough, "Environment-Aware Link Quality Prediction for Millimeter-Wave Wireless LANs," in Proc. ACM International Symposium on Mobility Management and Wireless Access, 2022.
- [13] G. Charan, A. Hredzak, C. Stoddard, B. Berrey, M. Seth, H. Nunez, and A. Alkhateeb, "Towards Real-World 6G Drone Communication: Position and Camera Aided Beam Prediction," in GLOBECOM 2022-2022 IEEE Global Communications Conference. IEEE, 2022, pp. 2951–2956.

- [14] S. Wu, M. Alrabeiah, A. Hredzak, C. Chakrabarti, and A. Alkhateeb, "Deep Learning for Moving Blockage Prediction using Real mmWave Measurements," in *ICC 2022-IEEE International Conference on Com*munications. IEEE, 2022, pp. 3753–3758.
- [15] G. Charan, M. Alrabeiah, and A. Alkhateeb, "Vision-aided dynamic blockage prediction for 6G wireless communication networks," in 2021 IEEE International Conference on Communications Workshops (ICC Workshops). IEEE, 2021, pp. 1–6.
- [16] J. Joo, M. C. Park, D. S. Han, and V. Pejovic, "Deep learning-based channel prediction in realistic vehicular communications," *IEEE Access*, vol. 7, pp. 27846–27858, 2019.
- [17] K. Ma, D. He, H. Sun, and Z. Wang, "Deep learning assisted mmWave beam prediction with prior low-frequency information," in *IEEE International Conference on Communications*. IEEE, 2021, pp. 1–6.
- [18] S. Zhang, A. Wijesinghe, and Z. Ding, "RME-GAN: a learning framework for radio map estimation based on conditional generative adversarial network," *IEEE Internet of Things Journal*, 2023.
- [19] K. He, Y. Huang, X. Chen, Z. Zhou, and S. Yu, "Graph attention spatial-temporal network for deep learning based mobile traffic prediction," in *IEEE Global Communications Conference (GLOBECOM)*. IEEE, 2019.
- [20] D. Wang, Y. Yang, and S. Ning, "DeepSTCL: A deep spatio-temporal ConvLSTM for travel demand prediction," in *International joint confer*ence on neural networks (IJCNN). IEEE, 2018, pp. 1–8.
- [21] K. He, X. Chen, Q. Wu, S. Yu, and Z. Zhou, "Graph attention spatial-temporal network with collaborative global-local learning for citywide mobile traffic prediction," *IEEE Transactions on Mobile Computing*, vol. 21, no. 4, pp. 1244–1256, 2020.
- [22] Q. Wu, K. He, X. Chen, S. Yu, and J. Zhang, "Deep transfer learning across cities for mobile traffic prediction," *IEEE/ACM Transactions on Networking*, vol. 30, no. 3, pp. 1255–1267, 2021.
- [23] J. Palacios, P. Casari, H. Assasa, and J. Widmer, "LEAP: Location estimation and predictive handover with consumer-grade mmWave devices," in *IEEE INFOCOM 2019-IEEE Conference on Computer Communications*. IEEE, 2019, pp. 2377–2385.
- [24] S. H. A. Shah, M. Sharma, and S. Rangan, "LSTM-based multi-link prediction for mmWave and sub-THz wireless systems," in ICC 2020-2020 IEEE International Conference on Communications (ICC), 2020.
- [25] A. Al-Saman, M. Cheffena, O. Elijah, Y. A. Al-Gumaei, S. K. Abdul Rahim, and T. Al-Hadhrami, "Survey of millimeter-wave propagation measurements and models in indoor environments," *Electronics*, vol. 10, no. 14, p. 1653, 2021.
- [26] "MmWave ray tracer for WLAN data generation." [Online]. Available: https://github.com/yuchen-sh/mmWave\_ray\_tracer
- [27] J. Lu, D. Steinbach, P. Cabrol, P. Pietraski, and R. V. Pragada, "Propagation characterization of an office building in the 60 GHz band," in *The 8th European Conference on Antennas and Propagation (EuCAP 2014)*. IEEE, 2014, pp. 809–813.
- [28] K. Sato, T. Manabe, T. Ihara, H. Saito, S. Ito, T. Tanaka, K. Sugai, N. Ohmi, Y. Murakami, M. Shibayama et al., "Measurements of reflection and transmission characteristics of interior structures of office building in the 60-GHz band," *IEEE transactions on antennas and propagation*, vol. 45, no. 12, pp. 1783–1792, 1997.
- [29] M. K. Samimi and T. S. Rappaport, "Characterization of the 28 GHz millimeter-wave dense urban channel for future 5G mobile cellular," NYU Wireless TR, vol. 1, 2014.
- [30] H. Assasa, J. Widmer, T. Ropitault, and N. Golmie, "Enhancing the ns-3 ieee 802.11 ad model fidelity: Beam codebooks, multi-antenna beamforming training, and quasi-deterministic mmwave channel," in Proceedings of the 2019 Workshop on ns-3, 2019, pp. 33–40.
- [31] G. TR, "Study on channel model for frequencies from 0.5 to 100 GHz," 2019.
- [32] D. Steinmetzer, D. Wegemer, M. Schulz, J. Widmer, and M. Hollick, "Compressive millimeter-wave sector selection in off-the-shelf IEEE 802.11 ad devices," in *Proceedings of the 13th International Conference* on emerging Networking Experiments and Technologies, 2017.
- [33] Z. Li, "Dataset for STAP framwork with environment dynamics." [Online]. Available: https://github.com/lzzz1998/moving-obj-data
- [34] R. Inc. [Online]. Available: https://www.remcom.com/ wireless-insite-em-propagation-software
- [35] C. Zhang, J. Li, Y. Zhao, T. Li, Q. Chen, X. Zhang, and W. Qiu, "Problem of data imbalance in building energy load prediction: Concept, influence, and solution," *Applied Energy*, vol. 297, p. 117139, 2021.
- [36] Z. Li, G. Xiong, Y. Chen, Y. Lv, B. Hu, F. Zhu, and F.-Y. Wang, "A hybrid deep learning approach with GCN and LSTM for traffic flow prediction," in *IEEE Intelligent transportation systems conference* (ITSC). IEEE, 2019, pp. 1929–1933.



Zhizhen Li received his bachelor degree from Nanjing University of Aeronautics and Astronautics, Nanjing, China in 2020 and master degree from school of Electrical Computer Engineering in Georgia Institute of Technology. He is currently a PhD student at North Carolina State University. His interest lies in wireless network and machine learning.



Mingzhe Chen (Member, IEEE) is currently an Assistant Professor with the Department of Electrical and Computer Engineering and Institute of Data Science and Computing at University of Miami. His research interests include federated learning, reinforcement learning, virtual reality, unmanned aerial vehicles, and Internet of Things. He has received four IEEE Communication Society journal paper awards including the IEEE Marconi Prize Paper Award in Wireless Communications in 2023, the Young Author Best Paper Award in 2021 and 2023,

and the Fred W. Ellersick Prize Award in 2022.



Gaolei Li (Member, IEEE) received the B.S. degree in electronic information engineering from Sichuan University, Chengdu, China, in 2015, and the Ph.D. degree in cyber security from Shanghai Jiao Tong University, Shanghai, China, in 2020. He is currently an Assistant Professor with the School of Electronic Information and Electrical Engineering, Shanghai Jiao Tong University. His research interests include adversarial machine learning and network security.



Xi Lin (Member, IEEE) received the B.S. degree from the School of Precision Instrument and Optoelectronics Engineering, Tianjin University, Tianjin, China, in 2016, and the Ph.D. degree in cyber security from Shanghai Jiao Tong University, Shanghai, China, in 2021. He is an Assistant Professor at the School of Electronic Information and Electrical Engineering, Shanghai Jiao Tong University. His research interests include blockchain, privacy computing, edge computing, and the Internet of Things.



Yuchen Liu (Member, IEEE) is currently an Assistant Professor with the Department of Computer Science at North Carolina State University, USA. He got his Ph.D. degree at the Georgia Institute of Technology, USA. His research interests include wireless networking, generative AI, distributed learning, mobile computing, and software simulation. He has received several best paper awards at IEEE and ACM conferences. He serves as Associate Editors of IEEE Transactions on Green Communications and Networking, Elsevier Computer Networks, and IEEE

Transactions on Machine Learning in Communications and Networking.